Journal of Power Sources 196 (2011) 9825–9829

Contents lists available at ScienceDirect

Journal of Power Sources

journal homepage: www.elsevier.com/locate/jpowsour

Short communication

Low temperature behaviour of TiO_2 rutile as negative electrode material for lithium-ion batteries

M. Marinaro[a,b], M. Pfanzelt[a], P. Kubiak[a,*], R. Marassi[b], M. Wohlfahrt-Mehrens[a]

[a] ZSW-Zentrum für Sonnenenergie und Wasserstoff-Forschung, Helmholtzstraße 8, D-89081 Ulm, Germany
[b] Camerino University, Department of Chemical Sciences, Via S. Agostino 1, Camerino 62032, Italy

ARTICLE INFO

Article history:
Received 4 May 2011
Received in revised form 21 June 2011
Accepted 5 July 2011
Available online 12 July 2011

Keywords:
Nanosized rutile TiO_2
Lithium insertion
Low temperature performance

ABSTRACT

High surface nanosized rutile TiO_2 is prepared via a sol–gel method from an ethylene glycol-based titanium-precursor in the presence of a non-ionic surfactant, at pH 0. Its electrochemical behaviour has been investigated at low temperature using two different potential windows. Typically, the potential window of the rutile system is 1–3 V but the use of an enlarged potential window (0.1–3 V), leads to an excellent reversible capacity of 341 mAh g^{-1} which is comparable to graphite anodes. The electrochemical performance was investigated by cyclic voltammetry and galvanostatic techniques at temperatures ranging from −40 to 20 °C. Nanosized TiO_2 exhibits excellent rate capability (341 mAh g^{-1} at 20 °C, 197 mAh g^{-1} at −10 °C, 138 mAh g^{-1} at −20 °C, and 77 mAh g^{-1} at −40 °C at a *C*/5 rate) and good cycling stability. The superior low-temperature electrochemical performance of nanosized rutile TiO_2 may make it a promising candidate as lithium-ion battery material.

© 2011 Elsevier B.V. All rights reserved.

1. Introduction

Lithium ion batteries are nowadays very popular and used in almost all portable electronic devices such as laptops, video cameras and mobile phones, and are being considered competitive candidates for alternative transportation. However, the future mass production of electrical vehicles (EV) and hybrid electrical vehicles (HEV) requires improvements of the battery technology in terms of performance, costs and safety as well as the development of alternative electrode materials. Since the late '80 s graphite has been the most common choice as the anode material for Li-ion batteries. The main drawbacks associated with use of graphite are related to its low rate capabilities and its poor electrochemical behaviour at low temperature [1–4]. The reduced ability of graphite to intercalate lithium into the structure at low temperatures has been attributed to factors such as the high charge-transfer resistance at the electrolyte–electrode interface, the low conductivity of the solid electrolyte interface (SEI) and the reduced solid state lithium diffusivity within graphene sheets at temperature below −20 °C. The past two decades have seen many efforts to improve the performance of carbon anodes at low temperature. Mild oxidation of graphite has proven to enhance performance and reduce the irreversible capacity loss [5–12]. Moreover, graphite mixed with metals/metal oxides nanoparticles dispersed in the carbon matrix, and graphite electrodes covered with a metal layer have shown improvements in the electrochemical behaviour at −20 and −30 °C [5,13–15]. Nevertheless, the development of alternative anode materials, with better performance at low temperature is still needed.

Due to their properties such as low cost, non-toxicity, high theoretical capacity (335 mAh g^{-1}), and a working voltage (1.4–1.8 vs. Li/Li^+) in the stability window of the most common electrolytes, titanates are promising candidates as alternative materials to carbonaceous anodes. Lithium insertion into bulk rutile is negligible at room temperature but it has been recently proven that a relevant amount of lithium can be inserted into nanosized rutile materials [16,17]. Theoretical studies on rutile-TiO_2 suggest that lithium insertion/deinsertion proceeds through two different paths: along the ab-plane ($D_{Li+} = 10^{-14}$ cm^2 s^{-1}) and via the *c*-axis ($D_{Li+} = 10^{-6}$ cm^2 s^{-1}) resulting in high anisotropy [18–20]. Thus, the control of the morphology of rutile nanoparticles appears as a key-point for efficient electrochemical behaviour. Earlier electrochemical studies on electrodes based on rutile TiO_2 reported high specific capacity and very good rate capabilities [21–26]. To the best of our knowledge, no results about low temperature performances of rutile-TiO_2 have been reported. In this work we evaluate the performance of nanosized rutile-TiO_2 electrodes in two different potential windows (0.1–3 and 1–3 V vs. Li^+/Li) in the temperature range $-40 \leq T\ (^\circ C) \leq 20$, and show that this material has good capacity retention over all the temperature range investigated.

* Corresponding author. Tel.: +49 (0)731 9530 401; fax: +49 (0)731 9530 666.
E-mail addresses: pierre.kubiak@zsw-bw.de, pkubiak@cicenergigune.com (P. Kubiak).

0378-7753/$ – see front matter © 2011 Elsevier B.V. All rights reserved.
doi:10.1016/j.jpowsour.2011.07.008

2. Experimental

2.1. Synthesis of nanosized rutile TiO_2

Rutile TiO_2 was synthesized by hydrolytic sol–gel route from a glycerol modified titanium precursor [27]. In a typical procedure 1.53 g (5.32 mmol) of sodium dodecyl sulphate (SDS, MERCK 85%) were dissolved in 250 ml of dilute hydrochloric acid (PROLABO, 32%) at pH 0, then 6.4 g of GMT (bis(1,2,3-trihydroxypropyl))titanate, prepared from titanium isopropoxide (Merck, 98%) and glycerol (Merck, 99%) were added to the solution, and treated in ultrasound bath at 60 °C for 2 h. After aging at 60 °C overnight the resulting powder was centrifuged, washed with water and dried at 60 °C overnight. Finally, the sample was heat-treated at 400 °C for 4 h in order to completely remove the surfactant.

2.2. Structural and morphological characterization

X-ray diffraction measurements were performed on a Siemens D5000 using Cu Kα radiation (λ = 0.154 nm). The crystallite size was evaluated with the Total Pattern Analysis (TOPAS) from Brucker and the volume-weighted full width at half-maximum (LVol-fwhm) adopting 0.6 as the sphericity value. The powder morphology was studied by scanning electron microscopy (SEM) using a Leo 1530 VP and by transmission electron microscopy (TEM) on a Titan 80–300 kV.

2.3. Electrodes preparation and electrochemical measurements

Electrodes were prepared starting from slurry of TiO_2:carbon Super P:PVdF in NMP with the mass ratio 76:12:12. After homogenizing by magnetic stirring, the slurry was spread onto a copper foil using Doctor Blade. The layer was first dried for 2 h at 40 °C and then over-night at 80 °C. Electrodes of 12 mm in diameter were punched, pressed and weighted before they were further dried under vacuum at 130 °C overnight. The average loading of all electrodes was ~2 mg cm^{-2}. Electrochemical measurements were carried out using T-shape 3-electrodes cells with stainless steel current collectors. Pure lithium foil was used both as the counter and the reference electrode. Glass microfiber was used as separator. A solution of 1 M $LiPF_6$ in EC:DMC:DEC 1:1:1 by volume was used as electrolyte. All the cells were assembled in a glove-box filled with Ar. For low temperature experiments cells were placed in a temperature chamber with T ranging from −40 °C to 20 °C (±0.1 °C). Li insertion/extraction into/from nanosized rutile TiO_2 electrodes was carried out for 5 cycles at $C/5$ for each investigated temperature. First, lithium was inserted/extracted at the highest temperature in order to get stable conditions, then the temperature was lowered and the cells equilibrated for at least 3 h prior to running the experiments. The reported capacities are extracted from the fifth cycle for each investigated temperature. Charge–discharge cycles and cyclic voltammograms were performed between two different potential windows (0.1–3 V and 1–3 V vs. Lithium) using a VMP (Bio-Logic, France) and Maccor systems. All the potentials are given vs. Li^+/Li redox couple; $1C = 0.335$ A g^{-1}.

3. Results and discussion

3.1. Synthesis and characterization

In this work nanoscale TiO_2 rutile has been synthesized via a hydrolytic sol–gel route from a glycerol-modified titanium precursor in presence of the anionic surfactant (SDS) at pH 0. The obtained solid was annealed at 400 °C/air for complete surfactant removal. X-ray Diffraction patterns collected from the synthesized TiO_2 are shown in Fig. 1. All the peaks could be ascribed to those of rutile phase. The crystallite size, determined using the Scherrer's formula, was found to be ~6 nm. The morphology of the samples was investigated by both SEM and HRTEM. The SEM image in Fig. 2 shows the micro-scale morphology of the rutile TiO_2. Cauliflower like aggregates with roughly spherical shapes are shown to be composed of whiskers organized in radial branches, thus forming nanowhisker arrays (insert in Fig. 2). HRTEM (Fig. 3) revealed that the rutile TiO_2 showed significant growth anisotropy, i.e. the whiskers revealed a high aspect ratio with diameters of approximately 4–5 nm, and lengths exceeding 40–50 nm. In addition, the specific surface area of the nanosized rutile TiO_2 has been determined by N_2-sorption. The material exhibits a rather high surface area of 180 m^2 g^{-1}. In summary, the applied synthesis protocol offers good control of the structure and morphology of TiO_2 rutile nanoparticles.

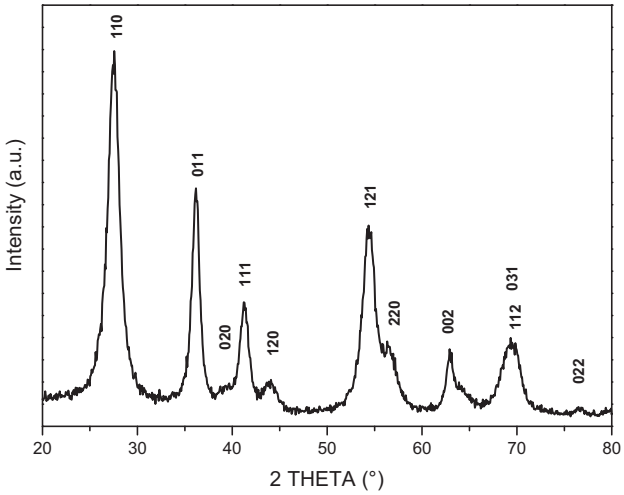

Fig. 1. X-Ray diffraction pattern of the synthesized rutile TiO_2.

3.2. Electrochemical performance

The electrochemical characterization of nanosized rutile has been carried out by both cyclic voltammetry and galvanostatic cycling. Cyclic voltammograms have been recorded between 1–3 V and 0.1–3 V vs. Li/Li^+ on nanosized rutile electrodes at a scan rate of 0.05 mV s^{-1}. The obtained voltammograms are presented in Fig. 4a and b. The first cycle shows two cathodic peaks at 1.4 and 1.1 V in both potential windows. These peaks can be ascribed to the irre-

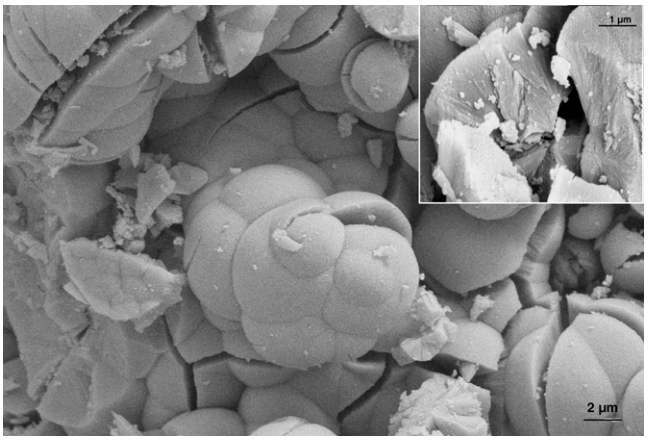

Fig. 2. Scanning electron microscopy images of the cauliflower-like rutile TiO_2 aggregates.

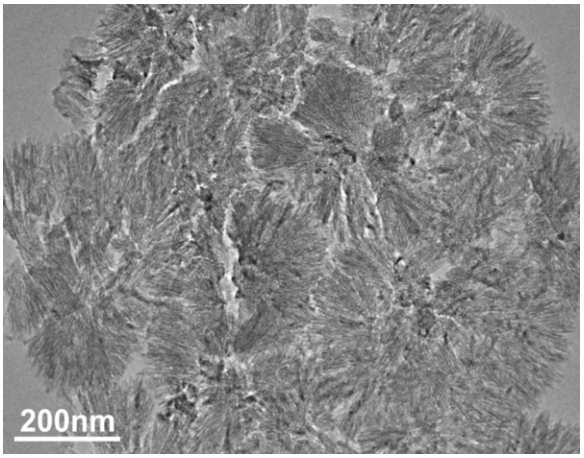

Fig. 3. HRTEM micrograph of the nanosized rutile TiO_2.

versible phase transformation from TiO_2 to $LiTiO_2$ [21,28,29]. The two other peaks observed below 1 V (Fig. 4b), are assigned to the irreversible reduction of the electrolyte [22,30]. The second and subsequent cycles exhibited reduction and oxidation peaks at about 1.8 V, which was consistent with lithium insertion/extraction in Li_xTiO_2.

The electrochemical behaviour of rutile TiO_2 at low temperature has been investigated by galvanostatic cycling between 1–3 V and 0.1–3 V. The evolution of the capacities with temperature is shown in Fig. 5, and the capacities extracted from the fifth cycle at each

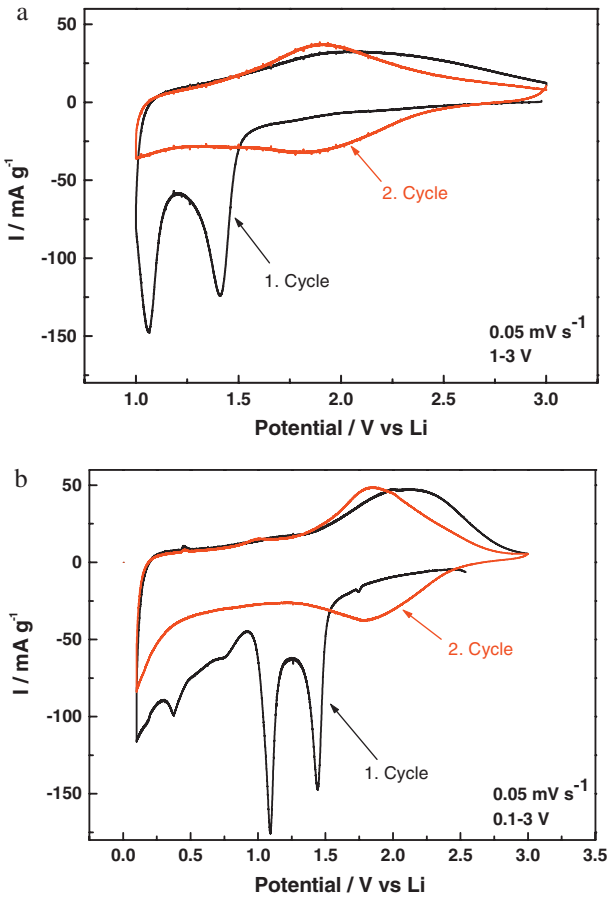

Fig. 4. Cyclic voltammograms of the TiO_2 rutile between 1 and 3 V (a) and 0.1–3 V vs. Li collected at room temperature with a scan rate of 0.05 mV s^{-1}.

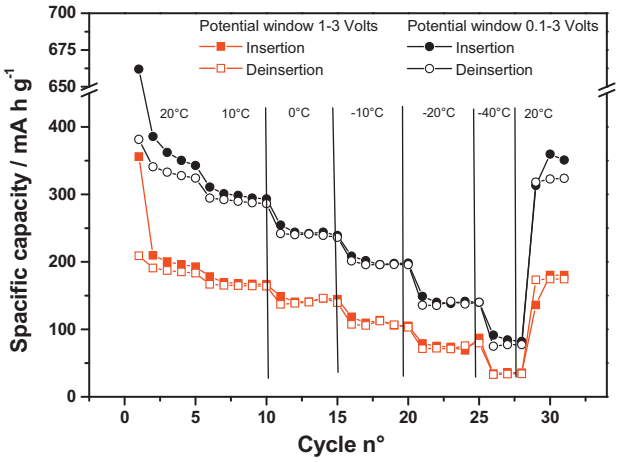

Fig. 5. Specific capacities obtained at different temperatures (*C*/5 rate) in two (0.1–3 V and 1–3 V) investigated potential windows.

investigated temperature are reported in Table 1. It can be seen that the reversible capacities progressively decrease with decreasing temperature. In the 1–3 V working potential window reversible capacities of 183, 140, 80 and 34 mAh g^{-1} are measured at 20, 0, −20 and −40 °C, respectively at *C*/5 charging rate. In our previous work we demonstrated that an enlargement of the potential limits to 0.1–3 V results in much higher reversible capacities. Indeed, by

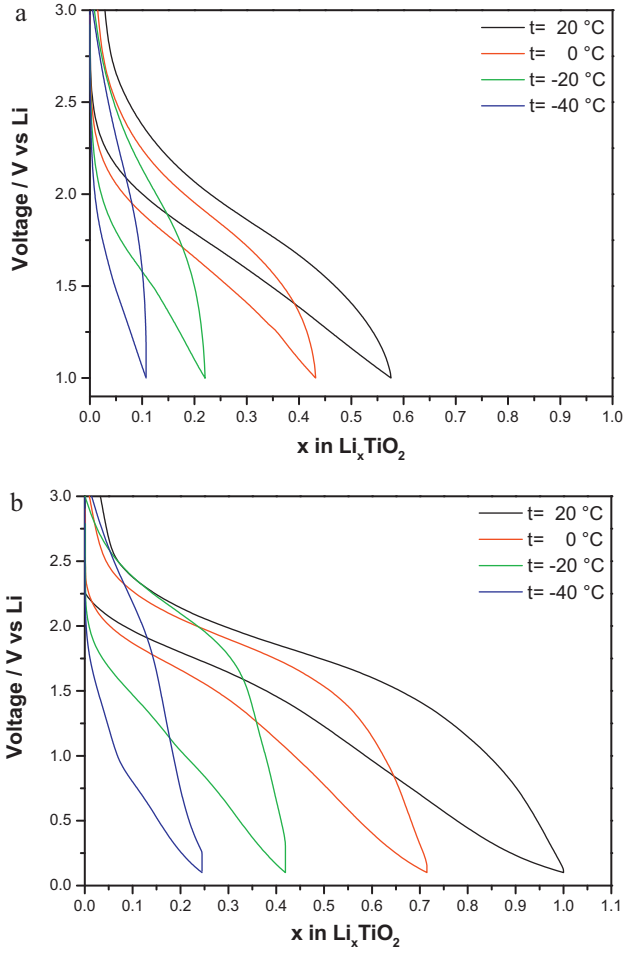

Fig. 6. Galvanostatic curves (*C*/5 rate) of rutile TiO_2 electrode at 20, 0, −20 and −40 °C recorded within 0.1–3 V (a) and 1–3 V (b) potential windows.

Table 1
Reversible capacities measured at different cycling temperatures for nanosized rutile TiO_2 (*C*/5 charge–discharge rate).

Temperature (°C)	Specific capacity (mAh g^{-1})	
	Pot. window 0.1–3 V vs. Li	Pot. window 1–3 V vs. Li
20	324	183
10	286	165
0	236	140
−10	196	103
−20	140	80
−40	77	34

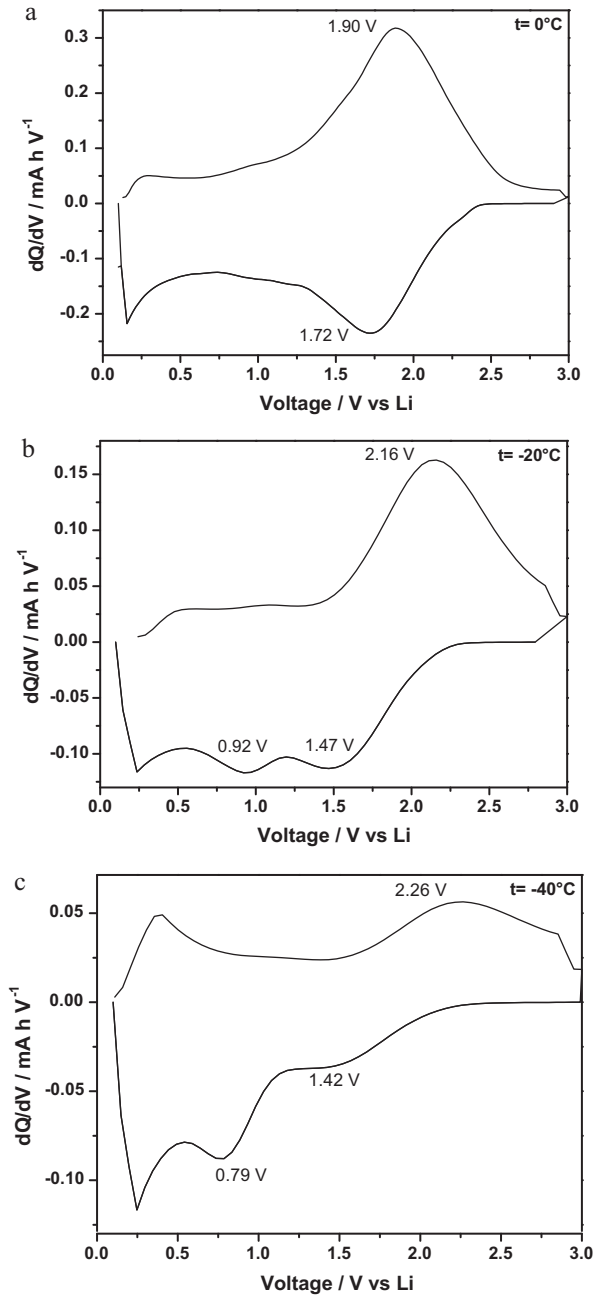

Fig. 7. Rate capability as function of the temperature for the 0.1–3 V (squares) and 1–3 V (circles) potential range.

using the 0.1–3 V potential window the reversible capacities at *C*/5 charging rate of rutile electrodes are 324, 240, 138 and 77 mAh g^{-1} at 20, 0, −20, and −40 °C, respectively. The capacities exhibited by the TiO_2 rutile electrodes at low temperature are higher than those reported for graphite. For example, a reversible capacity of only 26 mAh g^{-1} at −30 °C was achieved with mild oxidized graphite [13]. Moreover no lithium plating was observed on top of rutile electrodes after cycling at low temperature. Galvanostatic profiles, collected at four selected temperatures (20, 0, −20, −40 °C) are reported in Fig. 6a and b. The curves are extracted from the fifth cycle at the 4 studied temperatures. The charge–discharge cycles showed smooth sloped profile which is typical for a solid solution lithium insertion/extraction. It can be observed that the slope of the potential decay upon lithium insertion progressively increases with reducing the temperature. At −40 °C the potential dropped almost directly to 1 V and it could be seen that the insertion process takes place at potential below 1 V.

Differential capacity profiles d*Q*/d*V* vs. *E* (Fig. 7) were traced in the potential window 0.1–3 V for three different temperatures (0, −20, −40 °C) for a better understanding of the processes of low temperature lithium insertion/deinsertion. At 0 °C (Fig. 7a) only one pair of cathodic and anodic peaks at 1.72 and 1.90 V could be detected, the shape of the d*Q*/d*V* curve was similar to the second cycle of the cyclic voltammogram collected at RT (Fig. 4b). At −20 °C (Fig. 7b) the shape of the cathodic scan radically changed: two cathodic peaks were observed at 1.47 and 0.92 V on the reduction scan, whereas the oxidation part remained unchanged. The peak separation between the two cathodic peaks (1.42 and 0.79 V) was more pronounced at −40 °C (Fig. 7c). It appeared that the main lithium insertion took place at potential below 1 V. Moreover, the shape of the d*Q*/d*V* curves suggest a complex mechanism involving two processes with different kinetics. The exact nature of these electrochemical processes is still unclear and is the subject of further investigation.

Another aspect which must be considered is the influence of the Solid Electrolyte Interface (SEI) layer on the low temperature electrochemical performance of rutile TiO_2. For example, the low rate capabilities and poor low temperature electrochemical behaviour of graphite electrodes can be partly attributed to the presence of an SEI layer. In our previous work we demonstrated the effect of the SEI on the rate capabilities of rutile electrodes. A comparison of the TiO_2 rate capability at RT in the two different potential windows (0.1–3 V and 1–3 V) is reported in Fig. 8. It can be clearly seen, that the electrodes working in the smallest potential window (1–3 V) demonstrated the best rate capability while those measured in the

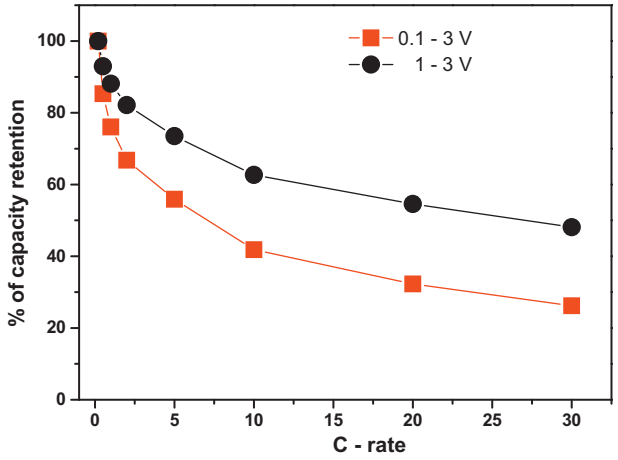

Fig. 8. TiO_2 rate capability at room temperature in the 0.1–3 V and 1–3 V potential windows.

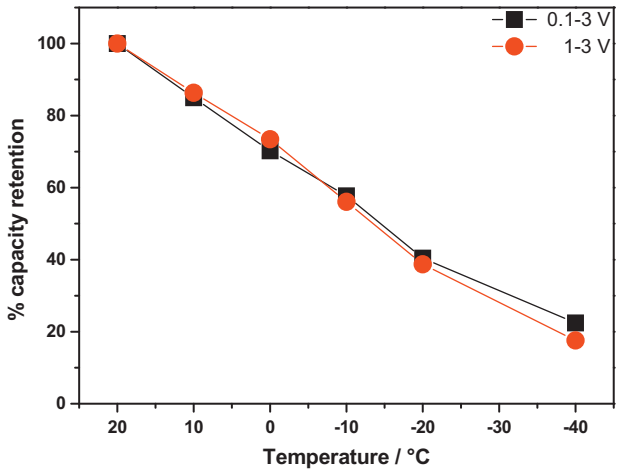

Fig. 9. Differential capacity curves for the 0.1–3 V potential window at different temperatures: (a) 0 °C, (b) −20 °C and (c) −40 °C.

0.1–3 V range exhibited the fastest decay. The rapid capacity decay when using the 0.1–3 V potential window was attributed to the presence of a SEI on top of rutile electrodes [22]. The same kind of comparison has been made for low temperature measurements. In Fig. 9 we report a comparison of the capacity retention as function of the temperature for both potential windows investigated. The capacity obtained at 20 °C was set as 100% for comparative reasons. The evolution of the capacity retention with the temperature followed the same trend in both potential windows. At −40 °C both electrodes showed capacity retention of about 20%. In the case of the 0.1–3 V potential window the negative effect of the SEI was compensated by the insertion of lithium at potentials <1 V. These results demonstrated the usefulness of using a large potential window for TiO_2 rutile to achieve good performance at low temperature.

4. Conclusion

Nanosized rutile-TiO_2 shows excellent electrochemical behaviour at low temperature. TiO_2 rutile electrodes are able to retain high capacity in both investigated potential windows (1–3 V and 0.1–3 V). As a result rutile-TiO_2 is able to insert ∼1 mol Li/TiO_2 at 20 °C, 0.7 mol Li/TiO_2 at 0 °C, 0.4 mol Li/TiO_2 at −20 and 0.25 mol Li/TiO_2 at −40 °C when cycled between 0.1 and 3 V vs. Li. The study of the differential profiles computed from the charge/discharge plots demonstrated that when the lower cut-off potential is placed at 1 V a relevant amount of the lithium insertion process is lost at low temperature. The obtained results open the way to new experiments with the purpose of better understanding the low temperature electrochemical behaviour of rutile. The superior performance shown by nanosized rutile-TiO_2 anodes makes this material a promising candidate for future lithium-ion batteries.

Acknowledgements

Financial support from Deutsche Forschungsgemeinschaft (DFG) within the Priority Program (SPP 1181) is gratefully acknowledged. The authors thank Prof. N. Hüsing and T. Fröschl, Ulm University, Institute of Inorganic Chemistry I, for the synthesis of the rutile TiO_2, Dr. U. Hörmann and Prof. U. Kaiser from the University of Ulm, Electron Microscopy Group of Material Science for the TEM measurement.

References

[1] C.K. Huang, J.S. Sakamoto, J. Wolfenstine, S. Surampudi, J. Electrochem. Soc. 147 (2000) 2893.
[2] S.S. Zhang, K. Xu, T.R. Jow, Electrochim. Acta 48 (2002) 241.
[3] H.P. Lin, D. Chua, M. Salomon, H.C. Shiao, M. Hendrickson, E. Plichta, S. Slane, Electrochem. Solid-State Lett. 4 (2001) A71.
[4] G. Nagasubramanian, J. Appl. Electrochem. 31 (2001) 1999.
[5] M. Mancini, F. Nobili, S. Dsoke, F. D'Amico, R. Tossici, F. Croce, R. Marassi, J. Power Sources 190 (2009) 141.
[6] E. Peled, C. Menachem, D. Bar-Tow, A. Melman, J. Electrochem. Soc. 143 (1996) L4.
[7] C. Menachem, E. Peled, L. Burstein, Y. Rosenberg, J. Power Sources 68 (1997) 277.
[8] C. Menachem, Y. Wang, J. Flowers, E. Peled, S.G. Greenbaum, J. Power Sources 76 (1998) 180.
[9] R.S. Rubino, E.S. Takeuchi, J. Power Sources 81–82 (1999) 373.
[10] T. Prem Kumar, A.M. Stephan, P. Thayananth, V. Subramanian, S. Gopukumar, N.G. Renganathan, M. Raghavan, N. Muniyandi, J. Power Sources 97–98 (2001) 118.
[11] N.A. Asrian, G.N. Bondarenko, G.I. Yemelianova, L.Y. Garlenko, O.I. Adrov, R. Marassi, V.A. Nalimova, D.E. Sklowski, Mol. Crystallogr. Liq. Crystallogr. 340 (2000) 331.
[12] X. Cao, J.H. Kim, S.M. Oh, Electrochim. Acta 47 (2002) 4085.
[13] F. Nobili, S. Dsoke, M. Mancini, R. Tossici, R. Marassi, J. Power Sources 180 (2008) 845.
[14] F. Nobili, M. Mancini, S. Dsoke, R. Tossici, R. Marassi, J. Power Sources 195 (2010) 7090.
[15] F. Nobili, S. Dsoke, T. Mecozzi, R. Marassi, Electrochim. Acta 51 (2005) 536.
[16] Y.S. Hu, L. Kienle, Y.G. Guo, J. Maier, Adv. Mater. 18 (2006) 1421.
[17] M.A. Reddy, M.S. Kishore, V. Pralong, V. Caignaert, U.V. Varadaju, B. Raveau, Electrochem. Commun. 8 (2006) 1299.
[18] F. Gligor, S.W. de Leeuw, Solid State Ionics 177 (2006) 2741.
[19] O.W. Johnson, Phys. Rev. 136 (1964) A284.
[20] M.V. Koudriachova, N.M. Harrison, S.W. deLeeuw, Phys. Rev. B65 (2002) 235423.
[21] P. Kubiak, M. Pfanzelt, J. Geserick, U. Hörmann, N. Hüsing, U. Kaiser, M. Wohlfahrt-Mehrens, J. Power Sources 194 (2009) 1099.
[22] M. Pfanzelt, P. Kubiak, M. Wohlfahrt-Mehrens, Electrochem. Solid-State Lett. 13 (A91) (2010).
[23] Y.-H. Hu, L. Kienle, Y.-G. Guo, J. Maier, Adv. Mater. 18 (2006) 1421.
[24] S. Bach, J.P. Pereira-Ramos, P. Willman, Electrochim. Acta 55 (2010) 4952.
[25] M. Anji Reddy, M. Satya Kishore, V. Pralong, V. Caignaert, U.V. Varadaraju, B. Raveau, Electrochem. Commun. 8 (2006) 1299.
[26] J.S. Chen, X.W. Lou, J. Power Sources 195 (2010) 2905.
[27] T. Ohzuku, Z. Takehara, S. Yoshizawa, Electrochem. Acta 24 (1979) 219.
[28] E. Baudrin, S. Cassaignon, M. Koesh, J.P. Jolivet, L. Dupont, J.M. Tarascon, Electrochem. Commun. 9 (2007) 337.
[29] M.A. Reddy, M.S. Kishore, V. Pralong, V. Caignaert, U.V. Varadaraju, B. Raveau, Electrochem. Commun. 8 (2006) 1299.
[30] M. Pfanzelt, P. Kubiak, M. Fleischhammer, M. Wohlfahrt-Mehrens, J. Power Sources (2010), doi:10.1016/j.jpowsour.2010.09.109.